Agricultural and Forest Meteorology 279 (2019) 107701

Contents lists available at ScienceDirect

Agricultural and Forest Meteorology

journal homepage: www.elsevier.com/locate/agrformet

An increasing trend in the ratio of transpiration to total terrestrial evapotranspiration in China from 1982 to 2015 caused by greening and warming

Zhongen Niu[a,b,c], Honglin He[a,b,d,*], Gaofeng Zhu[e], Xiaoli Ren[a,b,*], Li Zhang[a,b], Kun Zhang[f], Guirui Yu[a], Rong Ge[a,b,c], Pan Li[g], Na Zeng[a,b,c], Xiaobo Zhu[h]

[a] Key Laboratory of Ecosystem Network Observation and Modeling, Institute of Geographic Sciences and Natural Resources Research, Chinese Academy of Sciences, Beijing, 100101, China
[b] National Ecological Science Data Center, Institute of Geographic Sciences and Natural Resources Research, Chinese Academy of Sciences, Beijing, 100101, China
[c] University of Chinese Academy of Sciences, Beijing, 100049, China
[d] College of Resources and Environment, University of Chinese Academy of Sciences, Beijing, 100190, China
[e] Key Laboratory of Western China's Environmental Systems (Ministry of Education), College of Earth and Environmental Sciences, Lanzhou University, Lanzhou, 730000, China
[f] Institute of Tibetan Plateau Research, Chinese Academy of Sciences, Beijing, 100101, China
[g] Institute of Surface-Earth System Science, Tianjin University, Tianjin 300072, China
[h] Chongqing Engineering Research Center for Remote Sensing Big Data Application, School of Geographical Sciences, Southwest University, Chongqing, 400715, China

ARTICLE INFO

Keywords:
Transpiration to total terrestrial evapotranspiration ratio (T/ET)
Greening
Climate warming
Model-data fusion
PT-JPL model
Terrestrial ecosystem of China

ABSTRACT

The ratio of transpiration to total terrestrial evapotranspiration (T/ET) plays an important role in the hydrological cycle and in the energy budgets between the land and the atmosphere. Although China has experienced substantial climate warming and vegetation restoration (i.e., greening) over the past decades, the response of T/ET to the changing climate and environmental factors is poorly understood. Here, we apply a model-data fusion method that integrates the Priestly-Taylor Jet Propulsion Laboratory (PT-JPL) model with multivariate observational datasets (transpiration and evapotranspiration) to quantify the relative contributions of multiple factors to the T/ET trend for the terrestrial ecosystem of China from 1982 to 2015. Validation against the observational data indicates that the PT-JPL model performed well. The multi-year average T/ET was estimated to be 0.56 ± 0.05 in China. The T/ET of the forest ecosystems (0.65–0.72) was generally higher than that of the non-forest ecosystems (0.41–0.60). T/ET increased remarkably at a rate of 0.0019 yr^{-1} ($P < 0.01$) during the study period. Leaf area index increased significantly over the period, by 0.0031 $m^2 m^{-2} yr^{-1}$. It appears that greening and climate change were the most likely causes of the increasing T/ET in China, directly explaining 57.89% and 36.84% of the T/ET trend, respectively. Particularly, in the subtropical-tropical monsoonal region, greening directly contributed 24.43% to the T/ET trend whereas climate change contributed 60.95%. The influences of greening and climate change on T/ET trends are mutually reinforcing. Additionally, partial correlation analyses between the climate-driven T/ET and the climate variables indicate that warming (0.04 °C yr^{-1}, $P < 0.01$) was the major driving force of the climate-induced interannual variability of T/ET across the whole study area ($R = 0.84$), especially in the subtropical-tropical monsoonal region ($R = 0.89$). Our results may help elucidate the interactions between terrestrial ecosystems and the atmosphere within the context of long-term global climate changes.

1. Introduction

Evapotranspiration (ET) is a complex ecohydrological process that plays a pivotal role in the carbon cycle and energy budgets of the terrestrial ecosystems (Jung et al., 2010; Seneviratne et al., 2006). This process consists of biological transpiration (T), soil evaporation (ES), and canopy interception evaporation (EI) (Kool et al., 2014; Wang and Dickinson, 2012). An accurate quantification of the ratio of

* Corresponding authors at: Key Laboratory of Ecosystem Network Observation and Modeling, Institute of Geographic Sciences and Natural Resources Research, Chinese Academy of Sciences, Beijing, 100101, China.
E-mail addresses: hehl@igsnrr.ac.cn (H. He), renxl@igsnrr.ac.cn (X. Ren).

https://doi.org/10.1016/j.agrformet.2019.107701
Received 2 November 2018; Received in revised form 15 May 2019; Accepted 4 August 2019

transpiration to total terrestrial evapotranspiration (T/ET or T/(T + ES + EI)) is indispensable in the estimation of land water flux, which in turn can provide a deeper insight into the global interactions between the atmosphere and the terrestrial ecosystems (Lian et al., 2018). Quantifying the impact of changing environmental on T/ET is an important topic of research (Fisher et al., 2017). Over recent years, a wide range of approaches has been used to estimate T/ET (e.g., Jasechko et al., 2013; Maxwell and Condon, 2016; Lian et al., 2018), but none of these studies has quantified the relative contributions of multiple factors to the current terrestrial T/ET trend.

Of particular importance to water security and ecosystem management is the ability to quantify the impacts of multiple environmental factors to T/ET (Fisher et al., 2017). Several studies have focused on how T/ET responds to a range of biotic and abiotic variables (Granier et al., 1996; Kool et al., 2014; Good et al., 2015; Fatichi and Pappas, 2017; Li et al., 2019), but no uniform conclusion has been reached. For example, most studies have shown that vegetation plays a dominant role in evapotranspiration partitioning (e.g., Scanlon and Kustas, 2012; Wang et al., 2014; Zhou et al., 2016; Fatichi and Pappas, 2017), while other studies have found that the correlation between leaf area index (LAI) and T/ET is not statistically significant (Gu et al., 2018). Additionally, climate change, energy variability, CO_2 fertilization and other environmental factors are known to affect T/ET in ways that are inherently nonlinear and difficult to simulate (Loik et al., 2004; Moran et al., 2009; Bell et al., 2010; Costa et al., 2010; Schlesinger and Jasechko, 2014; Zhu et al., 2015; Li et al., 2018a; Stoy et al., 2019). Due to its large variability in climate and topography (Piao et al., 2005), China is ideal for investigating the responses of T/ET to environmental changes. Moreover, China's terrestrial ecosystem has experienced a complex set of dramatic changes in climate (e.g. climate warming) (Piao et al., 2010) as well as extensive vegetation greening (Piao et al., 2015; Li et al., 2018b) during the past few decades. These changes have profoundly altered the hydrological and physiological processes of the terrestrial ecosystems (Li et al., 2018b). Although a wide of studies highlight the significance of these environmental changes to terrestrial T/ET in China (e.g., Hu et al., 2009; Chang et al., 2014; Zhu et al., 2015; Song et al., 2018; Zhou et al., 2018), little is known about how concurrent changes of all of them have affected the T/ET trend of China's terrestrial ecosystem.

Previous research has improved our knowledge of T/ET, but its magnitude is still subject to debate (e.g., Wei et al., 2017; Jasechko et al., 2013; Kool et al., 2014; Zhou et al., 2016; Xiao et al., 2018; Talsma, 2018). For example, the isotope-based method produced T/ET higher than 70%, global land surface model estimated the T/ET to be approximately 50%, and hydrometric method calculated T/ET exceeding 50% (Sutanto et al., 2014). Although site measurements provide accurate local information on the T/ET ratio, their relative scarcity and inconsistent measurement (from only a few days or months up to years) precludes large scale up-scaling. Alternatively, models offer an effective way to derive T/ET estimates across temporal and spatial scales (Lian et al., 2018). By combining a set or sets of observations and a model, the model-data fusion method makes it possible to estimate model parameters and their respective uncertainties (Williams et al., 2009). Recently, the model-data fusion method has been increasingly used to optimize evapotranspiration model parameters and quantify model uncertainties based only on the observed evapotranspiration (Clark and Gelfand, 2006; García et al., 2013; Zhu et al., 2013, 2014a; Zhang et al., 2017; Gu et al., 2018). Those studies have remarkably improved the accuracy of overall evapotranspiration simulations; however, the combination with multiple parameters input to a deterministic model would generate large uncertainties in evapotranspiration partitioning (Reinds et al., 2008; Zhu et al., 2013). Therefore, simultaneous parameterization of evapotranspiration and transpiration in a deterministic model, based on observational evapotranspiration and transpiration data, is very essential for reducing the error in simulated T/ET. However, such studies are relatively rare (Zhu et al., 2014b).

With the rapid development of satellite technology, remote sensing-driven models have been widely used to estimate evapotranspiration and its partitioning (Cleugh et al., 2007; Mu et al., 2007; Fisher et al., 2008; Yao et al., 2013; Zeng et al., 2014; Liu et al., 2016; McCabe et al., 2019). Among these models, the Priestly-Taylor Jet Propulsion Laboratory (PT-JPL) model has been extensively used, due to its minimal requirements for local measurements (Fisher et al., 2008; Ershadi et al., 2014; McCabe et al., 2016; Zhu et al., 2016a) and that performed best among the four commonly used evapotranspiration models for most ecosystems and climate regions (Michel et al., 2016; Miralles et al., 2016). The PT-JPL model is considered to be effective for analyzing ET partitioning (Fisher et al., 2008; Gu et al., 2018).

The objective of this study is to investigate the T/ET trend in China for the period from 1982 to 2015. We first use observational transpiration and evapotranspiration data from multiple ecosystems to constrain the key parameters of the PT-JPL model, and then calculate T/ET using the optimized model parameters. Using simulation experiments of different scenarios and partial correlation analysis, we finally partition and attribute the T/ET trend to the changes in LAI, climate, and energy.

2. Methods and data

2.1. Methods

2.1.1. PT-JPL model

To overcome the uncertainty of the resistances in the Penman–Monteith equation, Priestley and Taylor (1972) designed a simple model for estimating potential evapotranspiration from wet surfaces (Yao et al., 2013). Based on four plant physiological constraints and one soil drought limitation, Fisher et al. (2008) developed the PT-JPL model for translating estimated potential evapotranspiration into actual evapotranspiration. In the PT-JPL model, ET has been partitioned into Soil evaporation (ES), interception evaporation (LE) and canopy transpiration (T). These are calculated as follows:

$$\mathrm{ET} = \mathrm{ES} + \mathrm{ET} + \mathrm{T} \tag{1}$$

$$\mathrm{ES} = (f_{\mathrm{wet}} + f_{\mathrm{SM}}(1 - f_{\mathrm{wet}}))\alpha\frac{\Delta}{\Delta + \gamma}(R_{\mathrm{ns}} - G) \tag{2}$$

$$\mathrm{EI} = f_{\mathrm{wet}}\alpha\frac{\Delta}{\Delta + \gamma}R_{\mathrm{nc}} \tag{3}$$

$$\mathrm{T} = (1 - f_{\mathrm{wet}})f_{\mathrm{g}}f_{\mathrm{T}}f_{\mathrm{M}}\alpha\frac{\Delta}{\Delta + \gamma}R_{\mathrm{nc}} \tag{4}$$

where α is the PT coefficient of 1.26 for a water body (unitless), Δ is the slope of the saturation-to-vapor pressure curve (kPa $^{\circ}C^{-1}$), γ is the psychrometric constant (0.066 kPa $^{\circ}C^{-1}$), G is ground heat flux (W m^{-2}), R_{nc} is the net radiation to the canopy (W m^{-2}), and is defined as $R_{\mathrm{nc}} = R_{\mathrm{n}} - R_{\mathrm{ns}}$, where R_{n} is the net radiation (W m^{-2}) and R_{ns} is the net radiation to the soil (W m^{-2}). R_{ns} can be calculated as $R_{\mathrm{ns}} = R_{\mathrm{n}}e^{-k_{\mathrm{Rn}}\mathrm{LAI}}$ (Fisher et al., 2008), where k_{Rn} is the extinction coefficient (unitless) (Impens and Lemur, 1969) and LAI is the leaf area index (m^2 m^{-2}). f_{wet} is the relative surface wetness, f_{SM} is the soil moisture constraint, f_{g} is the green canopy fraction, f_{T} is the plant temperature constraint, and f_{M} is the plant moisture constraint, these parameters are all unitless and calculated as follows:

$$f_{\mathrm{wet}} = RH^4 \tag{5}$$

$$f_{\mathrm{SM}} = RH^{VPD/\beta} \tag{6}$$

$$f_{\mathrm{g}} = f_{\mathrm{APAR}}/f_{\mathrm{IPAR}} \tag{7}$$

$$f_{\mathrm{T}} = e^{-((T_{\mathrm{a}} - T_{\mathrm{opt}})/T_{\mathrm{opt}})^2} \tag{8}$$

$$f_M = f_{APAR}/f_{APARmax} \quad (9)$$

where RH is relative humidity (%), VPD is saturation vapor pressure deficit (kPa),T_a is air temperature (°C), T_{opt} is optimum temperature for plant growth (°C), β is the sensitivity of the soil moisture constraint to VPD (kPa). f_{IPAR} is the fraction of photosynthetically active radiation (PAR) intercepted by canopy (unitless), and f_{APAR} is the fraction of PAR absorbed by canopy (unitless), $f_{APARmax}$ is the maximum f_{APAR}. To obtain a long-term sequence simulation of T/ET using the PT-JPL model, f_{IPAR} and f_{APAR} are defined as (Ruimy et al., 1999; Hatfield et al., 1984):

$$f_{APAR} = b_1(1 - e^{-k_1 \times LAI})$$

$$f_{IPAR} = b_2(1 - e^{-k_2 \times LAI})$$

where b_1, k_1, b_2, and k_2 are parameters. Seven parameters (Supplementary Table S1) in the PT-JPL model need to be estimated.

2.1.2. Global sensitivity analysis

Based on multi-source observational data (transpiration and evapotranspiration), Sobol's method (Sobol, 1990, 2001) is used to identify the sensitivity of parameters in the PT-JPL model. The model can be expressed as

$$y = f(X, \bar{\theta}) \quad (10)$$

where y represents the model output, X is the input variable, and $\bar{\theta}$ is the parameter vector. The total variance of function $V(y)$ for the multivariate datasets (transpiration and evapotranspiration) is defined as the product of the individual $V(y_i)$s:

$$V(y) = \prod_{i=1}^{I} V(y_i) \quad (11)$$

where $V(y_i)$ $(i = 1,2)$ can be decomposed into summands of increasing dimensionality (Zhang et al., 2017), which can be expressed by

$$V(y_i) = \sum_{m=1}^{K} V_{im} + \sum_{m=1}^{K-1} \sum_{n=m+1}^{K} V + \ldots + V \quad (12)$$

where V_{im} is the partial variance with the first-order index of θ_m on the model output y_i, V_{im} is the partial variance with the second-order index of the mth and nth parameter interactions of the ith data set, k is the length of parameters. In this method, the sensitivity effect is characterized by the ratio of the partial variances to the total variance (Zhang et al., 2013). See Supplementary Text S1 for details.

We categorized the sensitivity of the parameters as "highly sensitive", "sensitive", and "non-sensitive" when their contributions to the overall model output variance were > 10%, > 1%, and < 1%, respectively (Tang et al., 2006). In addition, a sample size of 10,000 was used to calculate the first-order and total-order sensitivity indices for the seven parameters of the PT-JPL model.

2.1.3. Parameter optimization with Differential Evolution Markov Chain

According to the Bayes theorem, the posterior probability of parameter sets θ can be written as

$$p(\theta|O) \propto p(O|\theta)p(\theta) \quad (13)$$

where O are the observed datasets, $p(\theta)$ is the prior probability distribution of parameter θ, $p(\theta|O)$ is the posterior probability distribution after Bayesian inference conditioned on available observations O, and $p(O|\theta)$ is the likelihood function, which reflects the influence of the observational datasets on parameter identification (Zhu et al., 2014a; Zhang et al., 2017).

For each dataset (evapotranspiration and transpiration), the model-data mismatch $\Delta_i(t)$ $(i = 1,2)$, which represents a relative "goodness-of-fit" measure for each possible parameter vector (van Oijen et al., 2011; Van Oijen et al., 2005), is expressed by

$$\Delta_i(t) = O_i(t) - f_i(t) \quad (14)$$

where $O_i(t)$ and $f_i(t)$ are observed and model estimated values of ith dataset at time t, respectively. The likelihood can be expressed as:

$$P(O_i(\cdot)|\theta) = \prod_{t=1}^{T_i} \frac{1}{\sqrt{2}\sigma_i} e^{-\frac{(\Delta_i(t))^2}{2\sigma_i^2}} \quad (15)$$

where T_i is the total length of observations of the ith data set, σ_i $(i = 1,2)$ is the standard deviation of the model error of the ith dataset (Braswell et al., 2005), and σ_i can be expressed as

$$\sigma_i = \sqrt{\frac{1}{T_i}\sum_{t=1}^{T_i}(\Delta_i(t))^2} \quad (16)$$

The likelihood function for multivariate data sets $p(O|\theta)$, used for parameter estimation is then defined as the product of the individual $p(O_i(\cdot)|\theta)$ (Richardson et al., 2010)

$$P(O|\theta) = \prod_{i=1}^{I} p(O_i(\cdot)|\theta) = \prod_{i=1}^{I}\prod_{t=1}^{T} \frac{1}{\sqrt{2}\sigma_i} e^{-\frac{(\Delta_i(t))^2}{2\sigma_i^2}} \quad (17)$$

where I is the number of datasets. The framework can be easily used when additional observations are available (Zhu et al., 2014b). In this study, the two datasets used to simultaneously optimize the parameter values were eddy covariance measured evapotranspiration and sap flow measured transpiration.

This method can reduce the prior uncertainties of the sensitive parameters and improve model accuracy (Gu et al., 2018). In this study, the coefficient of determination (R^2) and the root-mean-square-error (RMSE) were used to evaluate the model performance.

2.1.4. Simulation setup and analysis

To better understand the mechanisms controlling T/ET in the terrestrial ecosystem, we conducted seven simulations to examine the effects of three factors: LAI, climate and energy (Table 1). In our study, the climate effects included the influences of temperature and relative humidity. Energy effects referred to the impacts of net radiation.

To determine the relative importance of these three factors on terrestrial T/ET in China, we designed the following protocol. In the combined simulation (experiment 1, Table 1), we allowed all environmental factors to vary during the study period to determine the overall effects. In the following three simulations (experiments 2–4, Table 1), we held one of the driving environmental factors constant at an initial level, while allowing the others to change over time. Then, the effects of each environmental factor on terrestrial T/ET was quantified by calculating the difference in T/ET between the experiment where all factors changed over time and the experiment where the factor of interest was held constant. This approach captures both the direct effects of each environmental factor on terrestrial T/ET and the interactive effects of each factor with the other environmental factors. To examine the relative importance of interactive versus direct effects, we conducted another three simulations (experiments 5–7, Table 1) where only one of the environmental factors was allowed to change over time. Therefore, the direct effect of the LAI dynamic ('LAI Only'), climate change ('CLIM Only') and energy variability ('RAD Only') can be captured by the fifth, sixth and seventh experiment, respectively. The combined direct and

Table 1
Parameters and time periods used in each simulation experiment.

Experiment	LAI	Climate	Energy	Scenario
1	1982–2015	1982–2015	1982–2015	All Combined
2	1982	1982–2015	1982–2015	Combined without LAI
3	1982–2015	mean	1982–2015	Combined without Climate
4	1982–2015	1982–2015	mean	Combined without Radiation
5	1982–2015	mean	mean	LAI only
6	1982	1982–2015	mean	Climate only
7	1982	mean	1982–2015	Radiation only

"Climate" refers to temperature and relative humidity. "Energy" refers to net radiation.

interactive effects of the LAI dynamic ('LAI+'), climate change ('CLIM +') and energy vary ('RAD+') can be determined as the differences between the first and second scenarios, first and third scenarios, and first and fourth scenarios, respectively.

In addition, to compare the response of interannual variations in T/ET to annual temperature and precipitation, a partial correlation analysis was carried out on the results of scenario 6 in Table1. Regional mean T/ETs were calculated from regional mean transpiration and evapotranspiration values. The trend in regional T/ET was determined from the linear least squares regression of T/ET against year. Linear least squares regression method was also used to examine the slope of T/ET at the pixel scale.

2.2. Data

2.2.1. Observational data

In this study, water flux data (transpiration and evapotranspiration) from published literature were used to identify the sensitive parameters and evaluate the performance of the PT-JPL model across different biomes. The observational evapotranspiration data cover 15 forest sites, 15 grassland sites, 15 cropland sites, and 7 wetland sites (Zheng et al., 2016). Additional transpiration data for China were collected in this study, comprising 20 forest sites, 2 shrub sites, 3 cropland sites, and 1 grassland site (Fig. 1). We adopted the following methods to screen these data. First, transpiration flux data were measured using only the sap flow method at individual sites. However, the sap flow method is not applicable to grassland sites; therefore, for the grassland site, we inversed the data using the Hydrus-1D model, based on the site measurement data (Zhao et al., 2010). Second, we selected only those sites with at least 1 year of continuous flux measurements. Meanwhile, the data measured only during the growing season or longer than the growing season were used to represent the annual transpiration, because the contribution of transpiration during the winter to the annual transpiration is negligible. Detailed information for each site is listed in Supplementary Table S2. Furthermore, using a map of climatic regions in China (He et al., 2019), we classified the country into four climatic regions (i.e., high-cold Tibetan Plateau region (TP), temperate continental region (TCon), temperate monsoonal region (TMon), and subtropical-tropical monsoonal region (SubT)) to investigate responses of the terrestrial T/ET to environmental changes in different climatic regions

2.2.2. Remote sensing data

Remote sensing, which provides consistent LAI measurement datasets, has been widely used to monitor terrestrial vegetation growth (Piao et al., 2015). In this study, the arithmetic means of LAI from the Global Land Surface Satellite (GLASS) (Xiao et al., 2014, 2016) and Long-term Global Mapping (GLOBMAP) (Liu et al., 2012) data sets were used to assess vegetation growth. The GLASS LAI dataset was generated from AVHRR and MODIS reflectance data with general regression neural networks (Xiao et al., 2014). The temporal resolution of this dataset is 8 d and the spatial resolution is 0.05°. The GLOBMAP LAI dataset was constructed by merging the AVHRR LAI (1982–2000) with MODIS LAI (2000–2011) (Liu et al., 2012). The temporal resolution of GLOBMAP LAI is half a month during 1982–2000 and 8 d during 2001–2015, and the spatial resolution is 0.08°.

Repeated long-term satellite vegetation index measurements show a notable greening trend in the terrestrial ecosystem of China since 1982

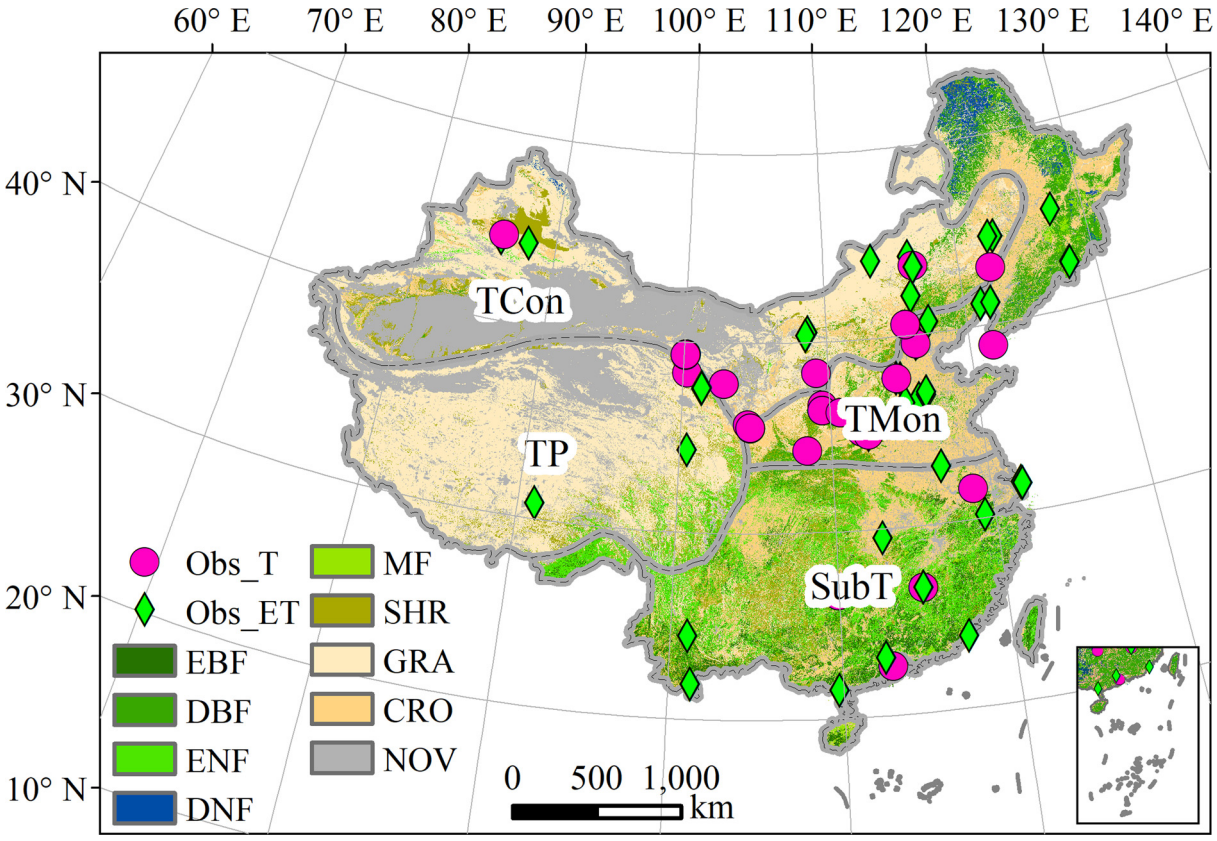

Fig. 1. Spatial distributions of sites for evapotranspiration (Obs_ET) and transpiration (Obs_T) observations in China. The base map reflects vegetation cover of China (Liu et al., 2002). EBF = evergreen broadleaf forest; DBF = deciduous broadleaf forest; ENF = evergreen needleleaf forest; DNF = deciduous needleleaf forest; MF = mixed forest; SHR = shrubland; GRA = grassland; and CRO = cropland. The division of climatic regions is from the China Natural Geography Atlas (He et al., 2019). TP = high-cold Tibetan Plateau region; TCon = temperate continental region; TMon = temperate monsoonal region; and SubT = subtropical-tropical monsoonal region.

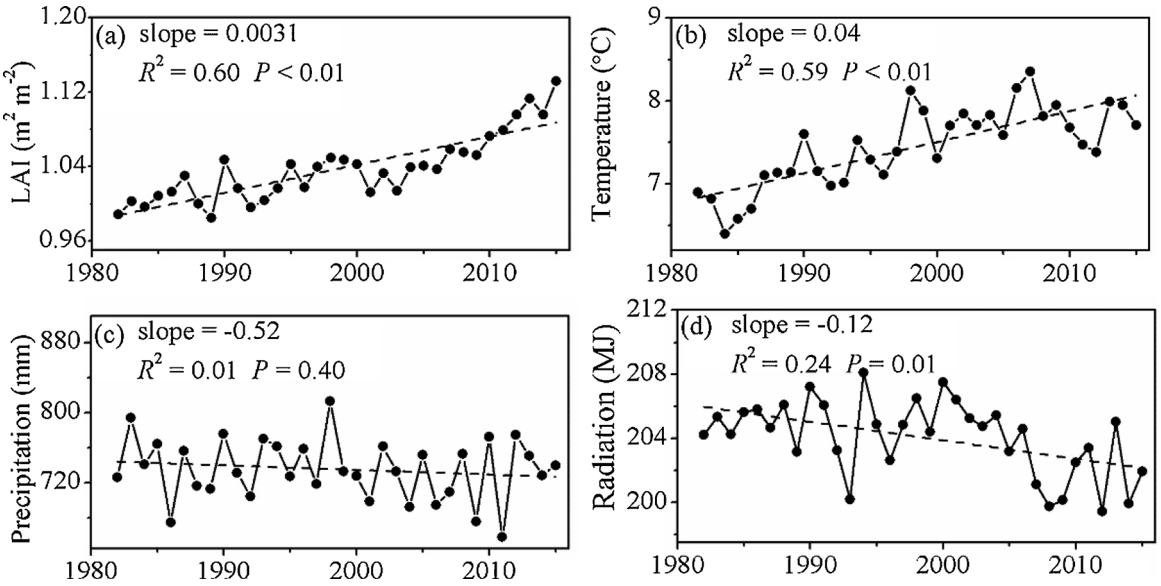

Fig. 2. Changes in (a) leaf area index (LAI), (b) annual mean temperature, (c) annual precipitation, and (d) annual net radiation in China for the period of 1982–2015.

(Piao et al., 2015). The annual increase in LAI was 0.0031 m^2 m^{-2} (P < 0.01) over the period 1982–2015, based on the forcing data used in this study (Fig. 2a).

2.2.3. Meteorological and energy data

We generated the gridded meteorological data (temperature, relative humidity and precipitation) from 1098 ground meteorological stations using ANUSPLIN interpolation computer software (Wang et al., 2017). The net radiation data were calculated from the FAO Penman model. Daily surface net radiation data for 53 radiation sites were used to optimize the model parameters, and then the net radiation data for 699 weather sites were calculated using the FAO Penman model and measurement data of these stations. Finally, the gridded net radiation data were obtained using ANUSPLIN interpolation computer software (Gao et al., 2013; Ren et al., 2018).

China has experienced significant climatic warming (Piao et al., 2010) and the annual temperature has increased by 0.04 °C yr^{-1} since 1982 (P < 0.01) (Fig. 2b), while annual precipitation has not changed significantly during this period (Fig. 2c). Moreover, net radiation in China has declined significantly during the past decades (Ren et al., 2018; Wild, 2009; Wild et al., 2009), with a decrease of 0.12 MJ yr^{-1} (P < 0.01) (Fig. 2d).

3. Results

3.1. Parameter optimization and validation

We use the observational transpiration and evapotranspiration data and Sobol's method to test the sensitivity indices of the PT-JPL model parameters across different ecosystems. Supplementary Figure S1 shows that four of the parameters, k_1, k_2, β and T_{opt}, are the most sensitive across various ecosystems, implying that these factors have the most influence on transpiration and evapotranspiration. T_{opt} has the highest first-order sensitivity indices in the forest and crop ecosystems (0.88 and 0.79, respectively), and β has the highest sensitivity indices in the shrub and grassland ecosystems (0.56 and 0.27, respectively).

We further use the Differential Evolution Markov Chain (DEMC) method to sample the posterior distributions of the sensitivity parameters (Supplementary Figure S2). The optimized β has a relatively low value (0.80) in the grassland ecosystem, suggesting that the surface constraint to the soil water content should be enhanced (Zhang et al., 2017). The T_{opt} parameter is highly correlated to the dynamic algorithms that we analyzed (Supplementary Figure S3), suggesting that our optimized values are reasonable. Variations in the optimized median k_1 and k_2 are large in the shrub ecosystem, mainly due to their relatively low sensitivities. Based on the posterior distributions of the sensitivity parameters, we tabulate the value of key parameters for the PT-JPL model for different ecosystems in the terrestrial ecosystem of China (Supplementary Table S3).

The accuracy of estimated T/ET depends on the accuracy of the simulated transpiration and evapotranspiration. Fig. 3 compares the model performance by using the optimized and original parameters with the directly observed transpiration and evapotranspiration data: the model using the optimized parameters performed better than that using the original parameters, especially for non-forest sites. For evapotranspiration, comparing all sites, forests sites and non-forest sites, the R^2 values increased from 0.67, 0.60, and 0.53 to 0.71, 0.68, and 0.64, respectively, and RMSE decreased from 209.54 mm yr^{-1}, 217.53 mm yr^{-1}, and 203.59 mm yr^{-1} to 153.57 mm yr^{-1}, 147.27 mm yr^{-1}, and 116.12 mm yr^{-1}, respectively (Fig. 3a). For transpiration, the optimized model also performed better than the original model, the R^2 value increased from 0.38 to 0.63 and RMSE decreased from 110.64 mm yr^{-1} to 68.12 mm yr^{-1} for all sites. For the non-forest sites in particular, the R^2 value increased remarkably, from 0.23 to 0.69, and RMSE decreased from 134.03 mm yr^{-1} to 72.46 mm yr^{-1} (Fig. 3b).

3.2. Spatial pattern of T/ET

The spatial pattern of mean annual T/ET for the period of 1982–2015 is shown in Fig. 4a. The annual T/ET is generally higher than 0.5 for the extensive monsoonal regions of China. Extensive forest cover, abundant precipitation, and high temperatures account for the high T/ET in these areas. In contrast, the annual T/ET is usually lower than 0.4 in the temperate-continental and high-cold Tibetan Plateau areas that are dominated by the alpine grasslands or deserts.

The multi-year average annual T/ET for the terrestrial ecosystems of China is 0.56 ± 0.05 (mean ± standard deviation) during the period of 1982–2015. The highest T/ET occurs in the subtropical-tropical monsoonal region (annual average 0.63 ± 0.06) followed by the temperate monsoonal region (annual average 0.60 ± 0.05), the temperate continental region (annual average 0.46 ± 0.07), and the high-cold Tibetan Plateau region (annual average 0.33 ± 0.03) (Fig. 4b).

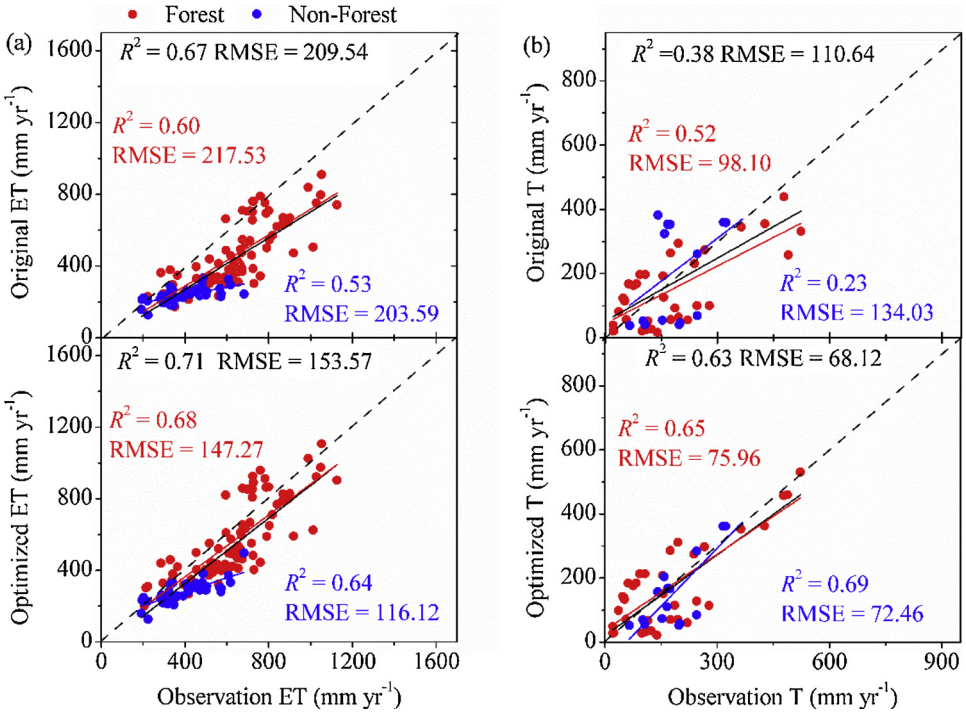

Fig. 3. Validation of the PT-JPL model based on observational (a) evapotranspiration and (b) transpiration data using original and optimized parameters. The black text in the figures indicated R^2 and RMSE of all sites; the red and blue points and text in the figures represent forest sites and non-forest sites, respectively. (For interpretation of the references to colour in this figure legend, the reader is referred to the web version of this article).

Meanwhile, T/ET varies widely among biomes. For example, forest ecosystems generally have higher annual T/ET than non-forest ecosystems (Supplementary Figure S4). Transpiration accounts for > 65% of the total evapotranspiration in forest ecosystems and the highest T/ET occurs in deciduous needleleaf forests (annual average 0.72 ± 0.15). For non-forest ecosystems, the annual average T/ET of the shrub ecosystem is almost 0.60, followed by croplands (annual average 0.55 ± 0.11). Grasslands have the lowest annual average T/ET (0.41 ± 0.09), which can be ascribed to the low vegetation cover.

3.3. T/ET trend

Fig. 5 shows the trend in T/ET during the period of 1982–2015 related to environmental changes. T/ET values that were estimated using the 'all combined' simulation scenario demonstrate a remarkable positive trend, with an annual increase of 0.0019 yr^{-1} ($P < 0.01$) (Fig. 5d). This significant increasing trend in T/ET is consistent for several regions ($P < 0.01$), and the largest annual increase in T/ET was found in the temperate continental region, with an increase of 0.0031 yr^{-1}. The annual increase in T/ET for the subtropical-tropical monsoonal, temperate monsoonal, and high-cold Tibetan Plateau regions is 0.0021 yr^{-1}, 0.0015 yr^{-1}, and 0.0014 yr^{-1}, respectively (Fig. 5e).

We investigate the direct contribution of the forcing factors to the T/ET trend using experiments 5 through 7. For the terrestrial ecosystems of China, the variation in LAI directly contributes 0.0011 yr^{-1} to the increase in T/ET ($P < 0.01$), accounting for about 57.89% of the T/ET trend using the 'all combined' simulation scenario (Fig. 5a). Historical climate variation also directly contributes substantially to the increase in T/ET (0.0007 yr^{-1}), explaining 36.84% of the variation in the T/ET trend (Fig. 5b). However, net radiation plays a minor role in the increasing T/ET trend. In the 'RAD Only' simulation scenario, the T/ET anomaly is nearly zero (Fig. 5c). Fig. 5e shows that LAI is the most important driving factor for the increasing T/ET trend, and climate variation is the second most influential factor for the increasing T/ET trend in the temperate continental and temperate monsoonal regions. In the high-cold Tibetan Plateau region, LAI also dominates the increasing T/ET trend, whereas climate variation reduces the slope of the T/ET trend. While in the subtropical-tropical monsoonal region, LAI directly

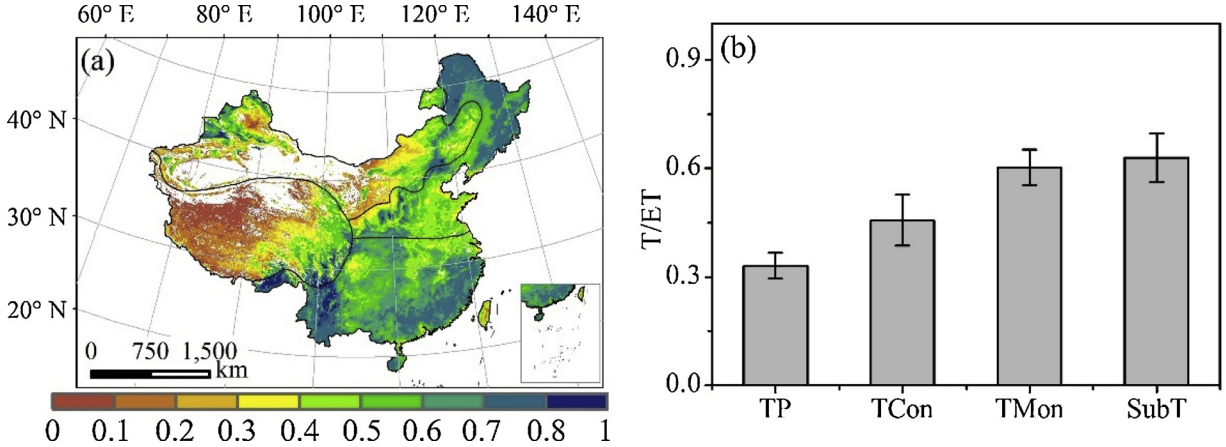

Fig. 4. (a) Spatial pattern of mean annual T/ET in the terrestrial ecosystem of China during the period of 1982–2015, and (b) mean annual average T/ET for each region.

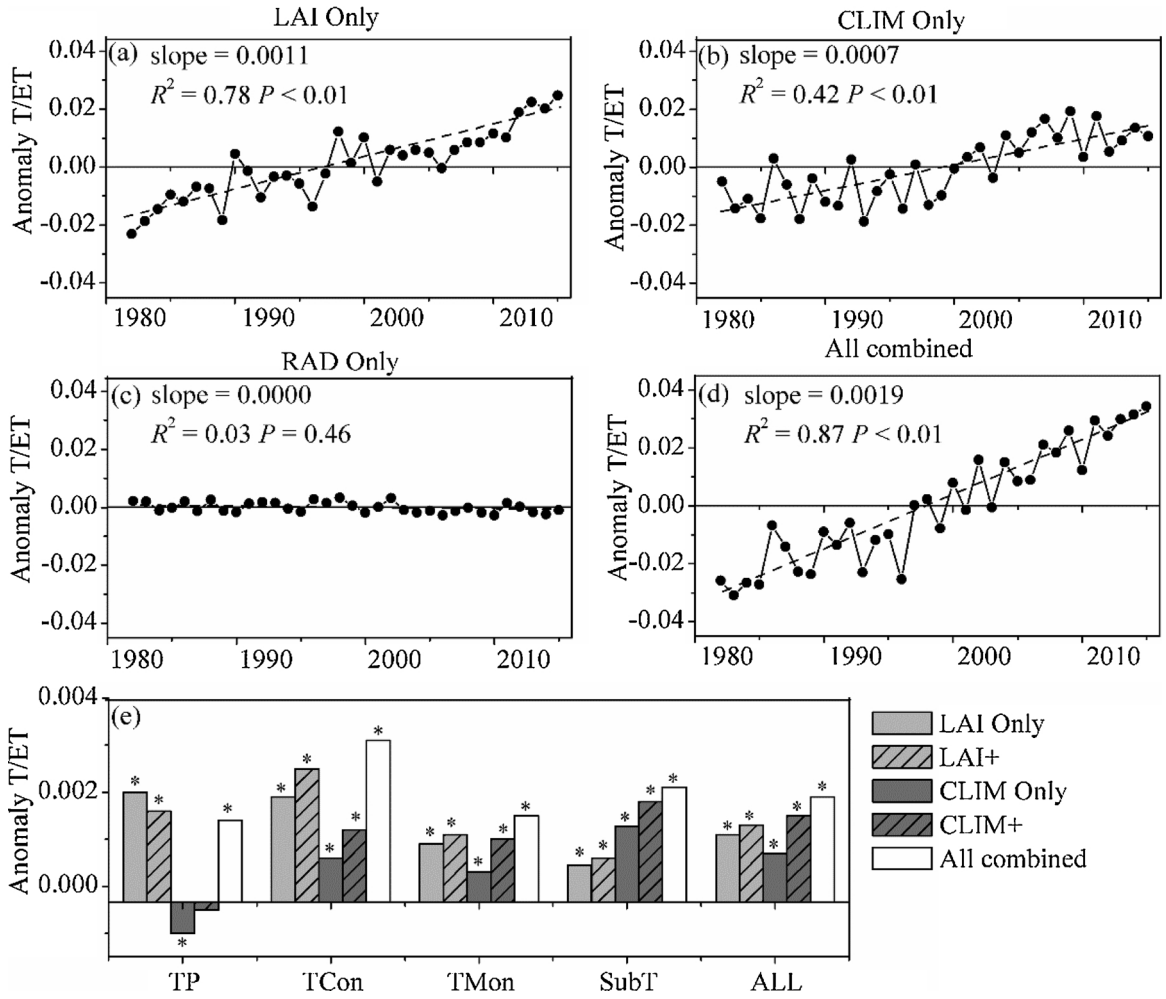

Fig. 5. Relative importance of environmental factors on the T/ET trend in China from 1982 to 2015. 'LAI only', 'CLIM only' and 'RAD only' represent the direct influence of LAI, climate, and energy, respectively. 'LAI+' and 'CLIM+' represent both the direct and interactive influences of LAI and climate.

contributes only 21.43%, and climate variation directly contributes 60.95% of the increasing T/ET trend. Net radiation has a negligible impact on the increasing T/ET trend in the different regions. This is also the case at the national scale.

LAI dynamic has an indirect effect on T/ET by enabling plants to be more responsive to climate change, and climate change also has an indirect effect on T/ET by promoting the effect of LAI (Fig. 5e). According to our analyses, increased LAI could lead to a larger effect of climate change on the T/ET trend (78.95%), than that resulting from climate change alone (36.84%), throughout the study area. Thus, climate change effects may vary from 36.84% to 78.95%, depending on the existence and magnitude of its interactions with LAI. Meanwhile, LAI dynamics also show a larger effect (68.42%) on T/ET trend when considering interactions with climate change, compared to their direct effects (57.89%). For the temperate-continental, temperate-monsoonal, and subtropical-tropical monsoonal regions, the effects of LAI dynamic and climate change on T/ET trends are mutually reinforcing, which consistent with the results of national scale. However, for the high-cold Tibetan Plateau region, the impacts of LAI and climate partly offset each other (Fig. 5e). The interactions among net radiation and the other environmental factors show negligible impact on the increasing T/ET trends; these interactions are not apparent in Fig. 5e.

The simulation scenarios 'LAI Only' and 'CLIM Only' both reveal that T/ET increased from 1982 to 2015. Nevertheless, these models differ in terms of transpiration and evapotranspiration. According to Fig. 6a, changes in LAI ('LAI Only') can lead to an increase in both evapotranspiration and transpiration. The increase in evapotranspiration (0.02%–0.06%) is lower than that in transpiration (0.04%–0.37%) for all regions. According to the 'CLIM Only' simulation, evapotranspiration in China is relatively stable from 1982 to 2015, with an annual increase of 0.03%, while transpiration rate increases by 0.26% yr^{-1} (Fig. 6b). Net radiation ('RAD Only') can cause evapotranspiration and transpiration to decrease by similar proportions across the whole study area (Fig. 6c). Overall, the 'All Combined' scenario indicates that environmental changes caused transpiration to increase (0.33% yr^{-1}) and reduced evapotranspiration (-0.04% yr^{-1}) across the whole study area. These results are mostly consistent with those for the temperate continental, temperate monsoonal, and subtropical-tropical monsoonal regions. Meanwhile, although changes in environmental factors can raise evapotranspiration and transpiration in the high-cold Tibetan Plateau region, the increase in evapotranspiration is lower than that in transpiration (Fig. 6d).

The spatial pattern of the sensitivities of the T/ET trend to LAI, climate, energy, and all drivers is shown in Fig. 7. LAI raised T/ET in 71% of the entire study area and increased it significantly in 42% ($P < 0.05$) of the study area. The temperate monsoonal region has the highest increase in T/ET. Meanwhile, T/ET declined in about 29% of the study area, mainly in northeastern China and part of the southwestern subtropical-tropical monsoonal region (Fig. 7a). On their own, climate factors raised T/ET in most parts of the temperate continental, temperate monsoonal, and subtropical-tropical monsoonal regions, but lowered it in the high-cold Tibetan Plateau region (Fig. 7b). Changes in

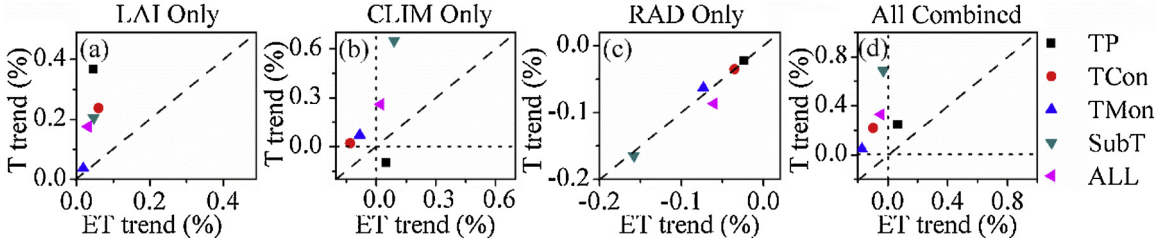

Fig. 6. Changes in evapotranspiration and transpiration rate according to (a) 'LAI Only', (b) 'CLIM Only', (c) 'RAD Only', and (d) 'All Combined' for the period of 1982–2015. Evapotranspiration and transpiration trends were normalized by their multi-year average values.

net radiation had much less effect on the T/ET trends than changes in either LAI or climate over the study period. The slope of the T/ET trend across the study area is between -0.002 and 0.002 (Fig. 7c). When the effect of all the drivers was combined, there is a positive T/ET trend in about 80% of the pixels and negative T/ET trend only in part of northeastern China and the high-cold Tibetan Plateau (Fig. 7d). We further analyzed the effect of different factors on evapotranspiration and transpiration and found that evapotranspiration and transpiration have different sensitivities to the changes in LAI, climate, and energy (Supplementary Figure S5).

To further investigate the effect of climatic variables on the increasing T/ET trend, we conducted a partial correlation analysis by comparing the annual T/ET series calculated from 'CLIM Only' with climatic conditions (mean annual temperature and annual cumulative precipitation) for China's terrestrial ecosystems during the period of 1982–2015 (Fig. 8). T/ET is significantly positively correlated with mean annual temperature (R = 0.84), while it is non-significantly negatively correlated with annual cumulative precipitation (R = -0.47) for the whole study area. The correlations between T/ET and climatic variables in the different regions are consistent with those for the whole country, especially in the subtropical-tropical monsoonal region (R = 0.89). This suggests that, both nationally and regionally, temperature change is the most important driver of the portion of interannual T/ET variation that could be ascribed to climate (Fig. 8).

The spatial pattern of the partial correlation coefficient between T/ET and climate variables for the entire country during the study period is shown in Fig. 9. More than 90% of the pixels show a positive correlation between temperature and T/ET variations. The highest partial correlation coefficient between T/ET and temperature is located mainly in the subtropical-tropical monsoonal regions (Fig. 9a). In contrast, precipitation and T/ET are negatively correlated for about 80% of the pixels of China, especially in the temperate and subtropical-tropical monsoonal regions. Additionally, the correlation between precipitation and T/ET is positive for parts of the high-cold Tibetan Plateau and temperate continental regions (Fig. 9b).

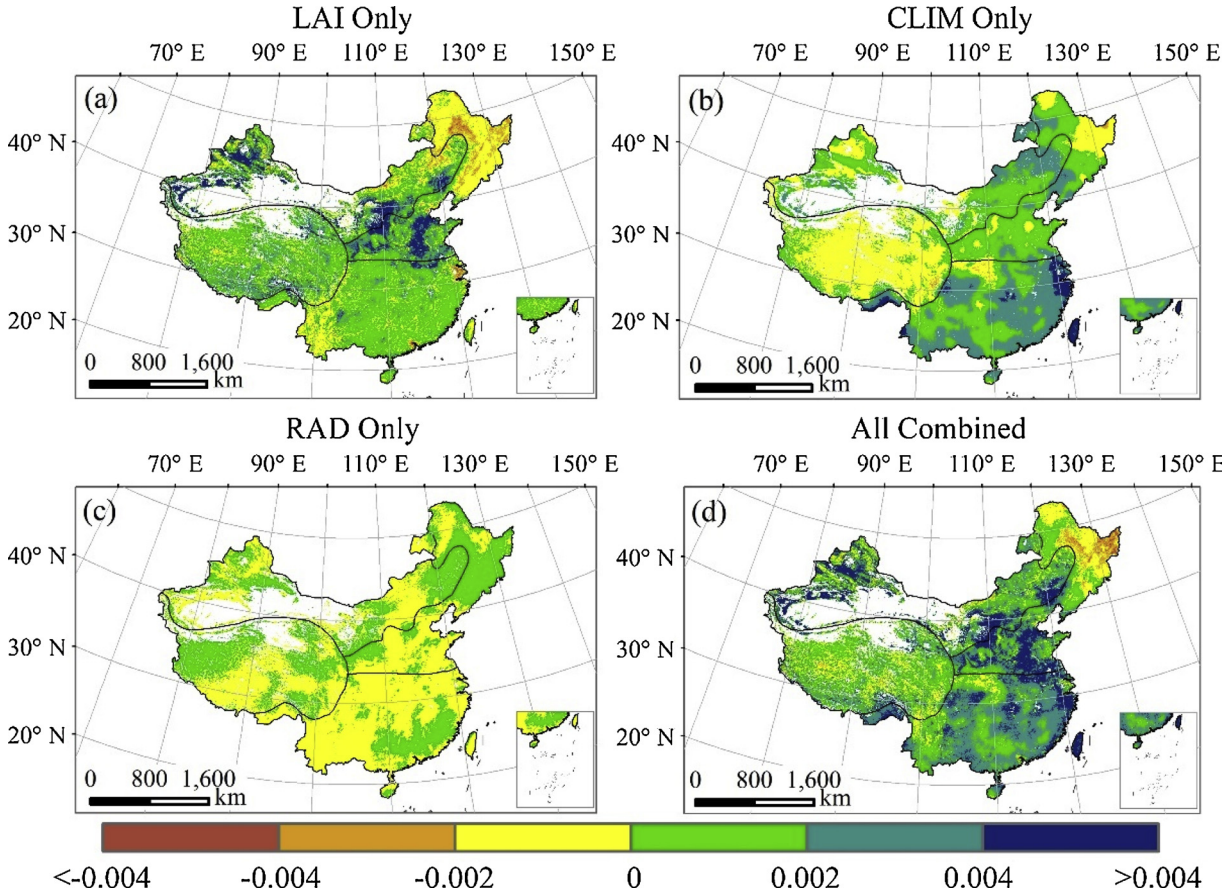

Fig. 7. Spatial pattern of simulated T/ET trend in the scenarios of (a) 'LAI Only', (b) 'CLIM Only', (c) 'RAD Only', and (d) 'ALL Combined' in China from 1982 to 2015.

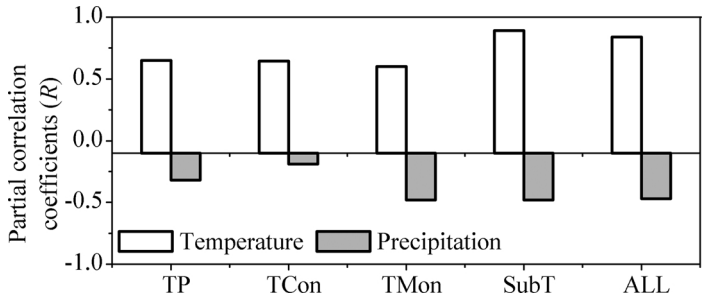

Fig. 8. Partial correlation coefficients between T/ET and climate factors for each region in China for the period of 1982–2015.

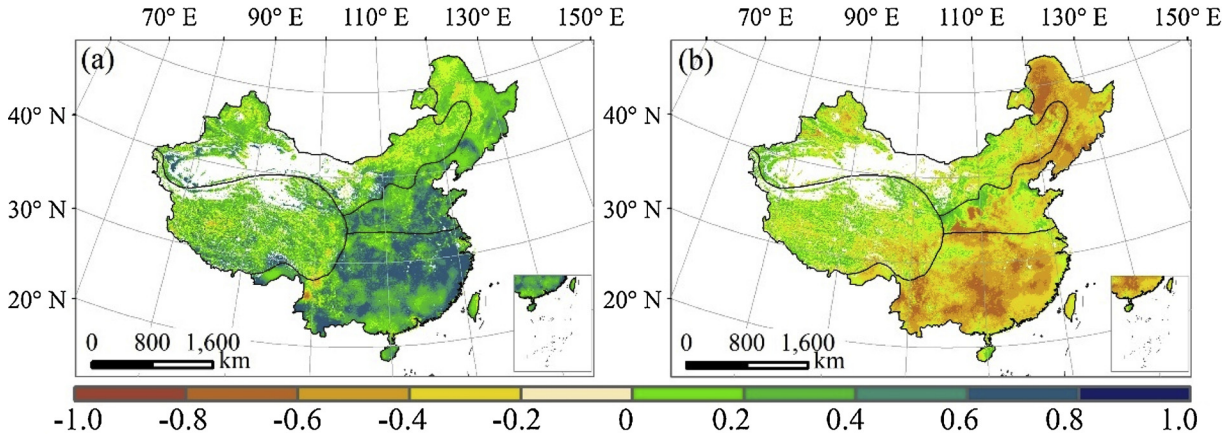

Fig. 9. Spatial pattern of the partial correlation coefficient between T/ET and (a) mean annual temperature and (b) annual cumulative precipitation in China from 1982 to 2015.

4. Discussion

Understanding the influence of model parameters on model response is essential to hydrological modeling (Brigode et al., 2013; McCabe et al., 2016). To obtain reliable estimated results, the key parameters of PT-JPL model are needed to optimize (Zhang et al., 2017). Previous studies focused on the model's sensitivity to forcing data (Fisher et al., 2008; García et al., 2013) or optimized the key parameters only based on observational evapotranspiration data (Zhang et al., 2017). Our study used a model-data fusion method to simultaneously parameterize the PT-JPL model against multivariate datasets (observational evapotranspiration and transpiration) to improve the accuracy of estimated T/ET, and found that four parameters (T_{opt}, k_1, k_2 and β) were sensitive to the transpiration and evapotranspiration simulation across different ecosystems, which was almost consistent with Zhang et al. (2017). T_{opt} was a basic parameter to the bio-constraint variable f_T and ranked first in the sensitivity index in forest and cropland ecosystems. In the original PT-JPL model, T_{opt} was dynamically calculated (Fisher et al., 2008), while that T_{opt} was unreliable in some specific biomes and climate conditions (García et al., 2013). Our study showed the optimized T_{opt} had better correlation to that calculated following Potter et al. (1993) (Supplementary Figure S3). The other bio-constraints (f_g and f_m) could be directly reflected by the sensitivity parameters k_1 and k_2. Additionally, β was more sensitive than other parameters in grassland and shrub ecosystems (Supplementary Figure S1), mainly because of that the soil received more energy than the canopy during the process of energy partition (Zhang et al., 2017), which indicated β had the most significant impacts on soil evaporation simulation and ET partition. The result is consistent with the previous finding that f_{SM} played a key role in model uncertainty in drylands (García et al., 2013). Although β was usually set as a unique constant parameter (Fisher et al., 2008; Mu et al., 2007), other studies argued that β should be fine-tuned in different regions (García et al., 2013; Zhang et al., 2017). Consistent with the previous study (Zhang et al., 2017), β was reduced in grassland ecosystem (Supplementary Figure S2 and Table S3), suggesting that the control of the soil moisture stress should be strengthened in dry ecosystem.

Based on the PT-JPL model using optimized parameters, the uncertainties in estimated transpiration and evapotranspiration were reduced. The model with optimized parameters showed better performance, and that was comparable to the performance achieved using models driven by climatic and remote sensing data. For evapotranspiration, the optimized model explained 71%, 68% and 64% of the variation for all sites, forest sites and non-forest sites, respectively, while the MODIS ET algorithm explained only 49%, 58%, and 32%, respectively (Niu et al., 2019). Moreover, the optimized PT-JPL model yielded an R^2 values close to those of the other models (e.g., RS-PM, BESS, SWH), for which the R^2 values are between 0.61 and 0.77 (e.g., Yuan et al., 2010; Li et al., 2014; Jiang and Ryu, 2016; Hu, 2017). Additionally, Chen et al. (2014) reported R^2 values of 0.5 to 0.8 for eight ET models at 23 eddy covariance sites. For transpiration, due to the limited amount of available transpiration measurement data, few studies have validated model performance at a large spatial scale. The accuracy of the optimized PT-JPL model is close to that of site-scale model. For example, the R^2 values of regressions between estimated transpiration and observational transpiration were 0.57–0.71 for forest and 0.13–0.83 for non-forest ecosystems, based on the empirical solar-induced chlorophyll fluorescence-based canopy conductance models (Shan et al., 2019); additionally, the R^2 values were 0.69–0.88 for cool temperate forest (Miyazawa et al., 2017). To further validate the model performance, we compared the estimated T/ET to the available field observation T/ET data in China, which we extracted from Lian et al. (2018) and Schlesinger and Jasechko (2014) (Supplementary Table S4); the R^2 value was 0.85 and the RMSE was 0.06 (Supplementary Figure S7). Therefore, despite the uncertainties, the accuracy of the PT-JPL model using the optimized parameters reaches that of the other models.

We further compared T/ET simulation results with T/ET results of previous studies and found that our estimated annual T/ET is almost within the range of those calculated by the process- and remote sensing-based models (Supplementary Text S2).

Our study provides a method to calculate T/ET at the ecosystem scale with results reflecting the characteristics of China's terrestrial ecosystems. The ratio of transpiration to evapotranspiration is influenced by vegetation morphology (Zhou et al., 2016), climate factors (Granier et al., 1996), air turbulence (Tuzet et al., 1997), and soil moisture availability (Shuttleworth and Wallace, 1985). Our study associates the T/ET trend with LAI dynamics, climate change, and energy variability.

Vegetation is the first-order factor affecting ET partitioning (Scanlon and Kustas, 2012). LAI is the primary factor controlling variations in T/ET (Lian et al., 2018; Zhu et al., 2016b; Berkelhammer et al., 2016; Fatichi and Pappas, 2017). The LAI dynamic not only determines the seasonal changes of T/ET (Li et al., 2019; Scott and Biederman, 2017; Zhu et al., 2015), but also determines most of the variability in annual T/ET across sites (Wang et al., 2014). An increase in LAI promotes canopy transpiration and interception evaporation by increasing the surface area, thereby leading to the rise in evapotranspiration (Li et al., 2018a; Piao et al., 2007). However, increased LAI usually reduces soil evaporation (Gu et al., 2018; Hu et al., 2009) mainly because its lowers the amount of energy (net radiation) reaching the soil surface (Hungate et al., 2002). The latter process may, in turn, offset the increase in evapotranspiration associated with high LAI (Huang et al., 2015). Therefore, transpiration and evapotranspiration may have different sensitivities to changes in LAI. The slopes of the correlations between transpiration and evapotranspiration and the LAI variables (as surrogates for the sensitivity of transpiration and evapotranspiration to changes in LAI) are illustrated in Supplementary Figure S8a, which might explain the relationship between the T/ET trend and greening. The sensitivity of transpiration to changes in LAI is much higher than that of evapotranspiration. Across the entire study area, transpiration and evapotranspiration increased by 18.04% and 3.07%, respectively, in response to the 0.1 $m^2 m^{-2}$ increase in LAI. Since transpiration is more sensitive to changes in LAI than evapotranspiration, greening (Fig. 2a and Supplementary Figure S9a) caused T/ET to increase over nearly the whole study area (Fig. 7a). A decrease in LAI in northeastern China (Supplementary Figure S9a) accounts in large part for the decreasing trend in T/ET in this region. Among the regions that were compared, transpiration is least sensitive to changes in LAI in the subtropical-tropical monsoonal region where evergreen forests are extensively distributed. A 0.1 $m^2 m^{-2}$ increase in LAI corresponds to only a 7.74% increase in transpiration in this area (Supplementary Figure S8a), mainly attributed to the offsets of the increase in interception evaporation caused by high LAI (Fatichi and Pappas, 2017).

Recent studies have shown that air temperature may affect T/ET by altering stomatal conductance at the site scale (Zhu et al., 2015), and that rising air temperature may raise the T/ET ratio (Zhu et al., 2014a). Higher temperatures can steepen the water potential gradient by lowering the relative humidity outside the leaf; the transpiration rate is therefore modulated by changes in water vapor pressure (Hopkins and Huner, 1999). Meanwhile, evapotranspiration also exhibits a rising tendency, mainly due to temperature-driven increases in the vapor pressure deficit (Bell et al., 2010; Li et al., 2018a). The effect of vapor pressure deficit on evapotranspiration is predicted to become increasingly important as global temperatures continue to rise (Novick et al., 2016). We compared the sensitivities of transpiration and evapotranspiration to temperature variation (Supplementary Figure S8b). Both transpiration and evapotranspiration, as estimated in experiment 6 (Table 1), increase with the rise in temperature. Nevertheless, the correlation between transpiration and temperature is stronger than that between evapotranspiration and temperature, especially in the subtropical-tropical monsoonal region. The influences of climate change and LAI dynamic on T/ET trends are mutually reinforcing. On one hand, climatic warming can promote vegetation growth by extending the growing season and simulating summertime photosynthesis (Niemand et al., 2005; Piao et al., 2008). Enhanced plant growth usually increases the leaf area, which would in turn cause T/ET to increase. On the other hand, increasing LAI would lead to an increase in transpiration area which could support greater canopy conductance (Stoy et al., 2019).

T/ET generally decreases with increasing precipitation (Moran et al., 2009; Reynolds et al., 2000), which is consistent with our results (Fig. 8). We ascribe this relationship to the fact that transpiration and evapotranspiration respond differently to increasing precipitation (Supplementary Figure S8c) (Gu et al., 2018). Meanwhile, the correlation between precipitation and T/ET is positive in parts of the high-cold Tibetan Plateau and temperate continental regions; these areas are relatively dry, hence, an increase in precipitation would cause T/ET to increase by promoting vegetation growth.

Net radiation determines the variation in evapotranspiration (Costa et al., 2010; Fisher et al., 2008; Zeng et al., 2014), and LAI controls how evapotranspiration is partitioned (Good et al., 2015; Wang et al., 2014; Wei et al., 2017). Therefore, changes in net radiation may not alter evapotranspiration partitioning if LAI remains unchanged. Meanwhile, previous studies found that the ratio of T/ET to the fraction of photosynthetically active radiation intercepted by the canopy is constant (about 1.2), suggesting that there is a relatively constant relationship between transpiration and intercepted radiation (Espadafor et al., 2015).

Our study follows a modeling approach to differentiate the effects of LAI, climate, and energy variability on T/ET. However, real-world ecosystems are affected by several other factors, especially increasing atmospheric CO_2 (Huang et al., 2015). The rise in atmospheric CO_2 could affect T/ET by causing stomatal closure and altering leaf area (Lian et al., 2018). Increased atmospheric CO_2 concentrations tend to reduce stomatal conductance based on leaf-level measurements (Sellers et al., 1996; Douville et al., 2000), and have been argued to decrease canopy conductance at continental scale (Gedney et al., 2006). However, CO_2 fertilization (the process whereby elevated CO_2 causes LAI to increase) could lead to an increase in the transpiration area; this could support greater canopy conductance, thereby compensating for the reduced canopy conductance resulting from increased atmospheric CO_2 (Stoy et al., 2019). The impact of elevated CO_2 has shown geographical variation. For temperate forests, transpiration was unaffected by elevated CO_2 because the greater canopy leaf area nullified the effect of leaf hydraulic acclimation on canopy conductance (Tor-ngern et al., 2015). However, in water limited ecosystems, which generally have relative low T/ET values, an increase in leaf area (which increases transpiration) compensates for stomatal closure (which reduces transpiration), thus creating a net transpiration increase (Lian et al., 2018; Woodward, 1990) and further leading to an increase in T/ET. In moist ecosystems with higher T/ET values, there is stronger suppression of transpiration as CO_2 increases (Lian et al., 2018). Although elevated CO_2 may reduce canopy conductance per unit area via light or hydraulic limitation, the potentially increasing leaf area leads to conserved transpiration (Schäfer et al., 2002; Ward et al., 2013), when the atmospheric demand for and soil supply of water remain unchanged, canopy transpiration and T/ET should decrease if the direct stomatal closure in response to elevated CO_2 cannot be countered by increased leaf area caused by CO_2 fertilization. In addition to being affected by rising atmosphere CO_2, LAI dynamic was also affected by the other factors, such as nitrogen deposition and afforestation (Piao et al., 2015; Zhu et al., 2015). The increasing T/ET caused by an increase in LAI was the combined result of various factors.

Although we have made progress in improving the accuracy of T/ET estimates by optimizing the sensitivity parameters, many uncertainties still affect the model outputs. The principal sources of model error might arise from the model structure and the inherent assumptions after the model parameters have been optimized by the DEMC method (Zhu

et al., 2014b). Uncertainty from the measured forcing data (Gu et al., 2018) and the observational data from the sap flow method and eddy covariance technique (Wilson et al., 2002, 2001) still may affect the accuracy of the estimated T/ET. Meanwhile, a spatial mismatch between the observational data and the satellite data also may reduce the accuracy of T/ET estimates (Fisher et al., 2008). In addition, this study was based only on the optimized PT-JPL model; in future, we will use multiple models to quantify the uncertainty in the PT-JPL model estimates.

5. Conclusions

This study used the PT-JPL model to calculate T/ET for the terrestrial ecosystems of China between 1982 and 2015. The T/ET trend and its drivers were further analyzed. A model-data fusion method was used to simultaneously parameterize the PT-JPL model against multivariate datasets (observed transpiration and evapotranspiration). We found that the PT-JPL model performs well for the terrestrial ecosystems of China. Validation data showed that the PT-JPL model explains 63% and 71% of the variation in observed transpiration and evapotranspiration, with RMSE values of 68.12 mm yr^{-1} and 153.57 mm yr^{-1}, respectively. The multi-year averaged T/ET for China is 0.56 ± 0.05. T/ET increased significantly during the study period, with an annual rise of 0.0019 yr^{-1} ($P < 0.01$). Greening and climate change explain 57.89% and 36.84% of the T/ET trend, respectively, whereas the contribution of energy change to the T/ET trend is negligible. Further, LAI dynamic has an indirect effect on T/ET by enabling plants to be more responsive to climate change, and climate change also has an indirect effect on T/ET by promoting the effect of LAI. In addition, partial correlation analyses between climate-only driven T/ET and the climate drivers show that temperature has the strongest influence on the interannual variations in T/ET ($R = 0.84$).

Acknowledgements

This work was supported by the National Key Research and Development Program of China (2016YFC0500204) and the Strategic Priority Research Program of the Chinese Academy of Sciences (XDA19020301).

Appendix A. Supplementary data

Supplementary material related to this article can be found, in the online version, at doi:https://doi.org/10.1016/j.agrformet.2019.107701.

References

Bell, J.E., Weng, E.S., Luo, Y.Q., 2010. Ecohydrological responses to multifactor global change in a tallgrass prairie: a modeling analysis. J. Geophys. Res-Biogeo 115, 12.
Berkelhammer, M., et al., 2016. Convergent approaches to determine an ecosystem's transpiration fraction. Global Biogeochem. Cycles 30 (6), 933–951.
Braswell, B.H., Sacks, W.J., E. L, Schimel, D.S., 2005. Estimating diurnal to annual ecosystem parameters by synthesis of a carbon flux model with eddy covariance net ecosystem exchange observations. Glob. Chang. Biol. 11 (2), 335–355.
Brigode, P., Oudin, L., Perrin, C., 2013. Hydrological model parameter instability: a source of additional uncertainty in estimating the hydrological impacts of climate change? J. Hydrol. 467 (7), 410–425.
Chang, X., et al., 2014. Qinghai spruce (Picea crassifolia) forest transpiration and canopy conductance in the upper Heihe River Basin of arid northwestern China. Agric. For. Meteorol. 198–199, 209–220.
Chen, Y., et al., 2014. Comparison of satellite-based evapotranspiration models over terrestrial ecosystems in China. Remote Sens. Environ. 140, 279–293.
Clark, J.S., Gelfand, A.E., 2006. A future for models and data in environmental science. Trends Ecol. Evol. 21 (7), 375–380.
Cleugh, H.A., Leuning, R., Mu, Q., Running, S.W., 2007. Regional evaporation estimates from flux tower and MODIS satellite data. Remote Sens. Environ. 106 (3), 285–304.
Costa, M.H., et al., 2010. Atmospheric versus vegetation controls of Amazonian tropical rain forest evapotranspiration: are the wet and seasonally dry rain forests any different? J. Geophys. Res. 115.
Douville, H., Planton, S., Royer, J.F., Stephenson, D.B., Tyteca, S., 2000. Importance of vegetation feedbacks in doubled-CO2 climate experiments. J. Geophys. Res. 105, 14841–14861.
Ershadi, A., McCabe, M.F., Evans, J.P., Chaney, N.W., Wood, E.F., 2014. Multi-site evaluation of terrestrial evaporation models using FLUXNET data. Agric. For. Meteorol. 187, 46–61.
Espadafor, M., Orgaz, F., Testi, L., Lorite, I.J., Villalobos, F.J., 2015. Transpiration of young almond trees in relation to intercepted radiation. Irrig. Sci. 33 (4), 265–275.
Fatichi, S., Pappas, C., 2017. Constrained variability of modeled T:ET ratio across biomes. Geophys. Res. Lett. 44 (13), 6795–6803.
Fisher, J.B., Tu, K.P., Baldocchi, D.D., 2008. Global estimates of the land–atmosphere water flux based on monthly AVHRR and ISLSCP-II data, validated at 16 FLUXNET sites. Remote Sens. Environ. 112 (3), 901–919.
Fisher, J.B., et al., 2017. The future of evapotranspiration: global requirements for ecosystem functioning, carbon and climate feedbacks, agricultural management, and water resources. Water Resour. Res. 53, 2618–2626.
Gao, Y.Z., et al., 2013. Spatial-temporal variation characteristics of surface net radiation in China over the past 50 years. J. Geo-Inf. Scie. 15 (1), 1–10.
García, M., et al., 2013. Actual evapotranspiration in drylands derived from in-situ and satellite data: assessing biophysical constraints. Remote Sens. Environ. 131, 103–118.
Gedney, N., et al., 2006. Detection of a direct carbon dioxide effect in continental river runoff records. Nature 439 (7078), 835.
Good, S.P., Noone, D., Bowen, G., 2015. Hydrologic connectivity constrains partitioning of global terrestrial water fluxes. Science 349 (6244), 175–177.
Granier, A., Huc, R., Barigah, S.T., 1996. Transpiration of natural rain forest and its dependence on climatic factors. Agric. For. Meteorol. 78 (1–2), 19–29.
Gu, C., et al., 2018. Partitioning evapotranspiration using an optimized satellite-based ET model across biomes. Agric. For. Meteorol. 259, 355–363.
Hatfield, J.L., Asrar, G., Kanemasu, E.T., 1984. Intercepted photosynthetically active radiation estimated by spectral reflectance. Remote Sens. Environ. 14, 65–75.
He, H.L., et al., 2019. Altered trends in carbon uptake in China's terrestrial ecosystems under the enhanced summer monsoon and warming hiatus. Sci. Rev., nuz021. https://doi.org/10.1093/nsr/nwz021.
Hopkins, W.G., Huner, N.P.A., 1999. Introduction to Plant Physiology. AIBS Bulletin, 10. John Wiley and Sons 39 pp.
Hu, Z.M., et al., 2009. Partitioning of evapotranspiration and its controls in four grassland ecosystems: application of a two-source model. Agric. For. Meteorol. 149 (9), 1410–1420.
Hu, Z.M., 2017. Modeling and partitioning of regional evapotranspiration using a satellite-driven water-carbon coupling model. Remote Sens. 9 (1), 54.
Huang, M., et al., 2015. Change in terrestrial ecosystem water-use efficiency over the last three decades. Glob. Chang. Biol. 21 (6), 2366–2378.
Hungate, B.A., et al., 2002. Evapotranspiration and soil water content in a scrub-oak woodland under carbon dioxide enrichment. Glob. Chang. Biol. 8 (3), 289–298.
Impens, I., Lemur, R., 1969. Extinction of net radiation in different crop canopies. Theor. Appl. Climatol. 17, 403–412.
Jasechko, S., et al., 2013. Terrestrial water fluxes dominated by transpiration. Nature 496 (7445), 347–350.
Jiang, C.Y., Ryu, Y., 2016. Multi-scale evaluation of global gross primary productivity and evapotranspiration products derived from Breathing Earth System Simulator (BESS). Remote Sens. Environ. 186, 528–547.
Jung, M., et al., 2010. Recent decline in the global land evapotranspiration trend due to limited moisture supply. Nature 467 (7318), 951–954.
Kool, D., et al., 2014. A review of approaches for evapotranspiration partitioning. Agric. For. Meteorol. 184, 56–70.
Li, X.L., et al., 2014. Estimation of evapotranspiration over the terrestrial ecosystems in China. Ecohydrology 7 (1), 139–149 2014.
Li, X.Y., et al., 2018a. Spatiotemporal pattern of terrestrial evapotranspiration in China during the past thirty years. Agric. For. Meteorol. 259, 131–140.
Li, Y., et al., 2018b. Divergent hydrological response to large-scale afforestation and vegetation greening in China. Sci. Adv. 4 (5), 9.
Li, X., et al., 2019. A simple and objective method to partition evapotranspiration into transpiration and evaporation at eddy-covariance sites. Agric. Forest Meterol. 265 (2019), 171–182.
Lian, X., et al., 2018. Partitioning global land evapotranspiration using CMIP5 models constrained by observations. Nat. Clim. Chang. 8 (7), 640–646.
Liu, J., et al., 2002. The land use and land cover change database and its relative studies in China. J. Geogr. Sci. 12 (3), 275–282.
Liu, S.M., et al., 2016. Upscaling evapotranspiration measurements from multi-site to the satellite pixel scale over heterogeneous land surfaces. Agric. For. Meteorol. 230, 97–113.
Liu, Y., Liu, R., Chen, J.M., 2012. Retrospective retrieval of long-term consistent global leaf area index (1981-2011) from combined AVHRR and MODIS data. J. Geophys. Res. Biogeosci. 117 (G4) n/a-n/a.
Loik, M.E., Breshears, D.D., Lauenroth, W.K., Belnap, J., 2004. A multi-scale perspective of water pulses in dryland ecosystems: climatology and ecohydrology of the western USA. Oecologia 141 (2), 269–281.
Maxwell, R.M., Condon, L.E., 2016. Connections between groundwater flow and transpiration partitioning. Science 353 (6297), 377–380.
McCabe, M.F., et al., 2016. The GEWEX LandFlux project: evaluation of model evaporation using tower-based and globally gridded forcing data. Geosci. Model. Dev. 9 (1), 283–305.
McCabe, M., Miralles, D., Holmes, T., Fisher, J., 2019. Advances in the Remote Sensing of Terrestrial Evaporation. Remote Sens. 11 (9) 1138–1138.
Michel, D., et al., 2016. The WACMOS-ET project - Part 1: tower-scale evaluation of four remote-sensing-based evapotranspiration algorithms. Hydrol. Earth Syst. Sci. 20 (2), 803–822.

Miralles, D.G., et al., 2016. The WACMOS-ET project – Part 2: evaluation of global terrestrial evaporation data sets. Hydrol. Earth Syst. Sci. 20 (2), 823–842.
Miyazawa, Y., et al., 2017. Transpiration of trees in a cool temperate forest on Mt. Aso, Japan: comparison of model simulation and measurements. Ecol. Res. 32 (4), 547–557.
Moran, M.S., et al., 2009. Partitioning evapotranspiration in semiarid grassland and shrubland ecosystems using time series of soil surface temperature. Agric. For. Meteorol. 149 (1), 59–72.
Mu, Q., Heinsch, F.A., Zhao, M., Running, S.W., 2007. Development of a global evapotranspiration algorithm based on MODIS and global meteorology data. Remote Sens. Environ. 111 (4), 519–536.
Niemand, C., Köstner, B., Prasse, H., Grünwald, T., Bernhofer, C., 2005. Relating tree phenology with annual carbon fluxes at Tharandt forest. Meteorol. Z. 14 (2), 197–202.
Niu, Z.E., et al., 2019. The spatial-temporal patterns of evapotranspiration and its influencing factors in Chinese terrestrial ecosystem from 2000 to 2015. Acta Ecol. Sin. 2019 (13). https://doi.org/10.5846/stxb201803090467. (in Chinese).
Novick, K.A., et al., 2016. The increasing importance of atmospheric demand for ecosystem water and carbon fluxes. Nat. Clim. Chang. 6 (11), 1023.
Piao, S., et al., 2010. The impacts of climate change on water resources and agriculture in China. Nature 467 (7311), 43.
Piao, S., et al., 2005. Changes in vegetation net primary productivity from 1982 to 1999 in China. Global Biogeochem. Cycles 19 (2) n/a-n/a.
Piao, S., et al., 2007. Changes in climate and land use have a larger direct impact than rising CO2 on global river runoff trends. Proc. Natl. Acad. Sci. U. S. A. 104 (39), 15242–15247.
Piao, S.L., et al., 2008. Net carbon dioxide losses of northern ecosystems in response to autumn warming. Nature 451 (7174), 49–U3.
Piao, S.L., et al., 2015. Detection and attribution of vegetation greening trend in China over the last 30 years. Glob. Chang. Biol. 21 (4), 1601–1609.
Potter, C.S., et al., 1993. Terrestrial ecosystem production: a process model based on global satellite and surface data. Global Biogeochem. Cycles 7 (4), 811–841.
Priestley, C.H.B., Taylor, R.J., 1972. On the assessment of surface heat flux and evaporation using large-scale parameters. Mon. Weather. Rev. 100 (2), 81–92.
Reinds, G.J., van Oijen, M., Heuvelink, G.B.M., Kros, H., 2008. Bayesian calibration of the VSD soil acidification model using European forest monitoring data. Geoderma 146 (3), 475–488.
Ren, X., He, H., Zhang, L., Yu, G., 2018. Global radiation, photosynthetically active radiation, and the diffuse component dataset of China, 1981–2010. Earth Syst. Sci. Data Discuss. 10 (3), 1217–1226.
Reynolds, J.F., Kemp, P.R., Tenhunen, J., 2000. Effects of long-term rainfall variability on evapotranspiration and soil water distribution in the Chihuahuan Desert: a modeling analysis. Plant Ecol. 150, 145–159.
Richardson, A.D., et al., 2010. Estimating parameters of a forest ecosystem C model with measurements of stocks and fluxes as joint constraints. Oecologia 164 (1), 25–40.
Ruimy, A., et al., 1999. Comparing global models of terrestrial net primary productivity (NPP): analysis of differences in light absorption and light-use efficiency. Glob. Chang. Biol. 5 (S1), 56–64.
Scanlon, T.M., Kustas, W.P., 2012. Partitioning evapotranspiration using an eddy covariance-based technique: improved assessment of soil moisture and land–atmosphere exchange dynamics. Vadose Zone J. 11 (3), 0.
Schäfer, R., Oren, R., Lai, C.T., Katul, G.G., 2002. Hydrologic balance in an intact temperate forest ecosystem under ambient and elevated atmospheric CO2 concentration. Glob. Chang. Biol. 8 (9), 895–911.
Schlesinger, W.H., Jasechko, S., 2014. Transpiration in the global water cycle. Agric. For. Meteorol. 189, 115–117.
Scott, R., Biederman, J., 2017. Partitioning evapotranspiration using long-term carbon dioxide and water vapor fluxes. Geophys. Res. Lett. 44 (13), 6833–6840.
Sellers, P.J., et al., 1996. Comparison of radiative and physiological effects of doubled atmospheric CO2 on climate. Science 271, 1402–1406.
Seneviratne, S.I., Luthi, D., Litschi, M., Schar, C., 2006. Land-atmosphere coupling and climate change in Europe. Nature 443 (7108), 205–209.
Shan, N., et al., 2019. Modeling canopy conductance and transpiration from solar-induced chlorophyll fluorescence. Agric. For. Meterol. 265 (15), 189–201.
Shuttleworth, W.J., Wallace, J., 1985. Evaporation from sparse crops-an energy combination theory. Q. J. R. Meteorol. Soc. 111 (469), 839–855.
Sobol, I.M., 1990. On Sensitivity Estimation For Nonlinear Mathematical Models. Keldysh Applied Mathematics Institute 2 (1), 112–118.
Sobol, I.M., 2001. Global sensitivity indices for nonlinear mathematical models and their Monte Carlo estimates. Math. Comput. Simul. 55 (1), 271–280.
Song, L., et al., 2018. Canopy transpiration of Pinus sylvestris var. Mongolica in a sparse wood grassland in the semiarid sandy region of Northeast China. Agric. For. Meteorol. 250–251, 192–201.
Stoy, P.C., et al., 2019. Reviews and syntheses: turning the challenges of partitioning ecosystem evaporation and transpiration into opportunities. Biogeosci. Discuss. https://doi.org/10.5194/bg-2019-85. in review.
Sutanto, S.J., et al., 2014. HESS Opinions "A perspective on isotope versus non-isotope approaches to determine the contribution of transpiration to total evaporation. Hydrol. Earth Syst. Sci. 18 (8), 2815–2827.
Talsma, C., et al., 2018. Partitioning of evapotranspiration in remote sensing-based models. Agric. For. Meteorol. 260–261, 131–143.
Tang, Y., Reed, P.M., Wagener, T., Van Werkhoven, K.L., 2006. Comparing sensitivity analysis methods to advance lumped watershed model identification and evaluation. Hydrol. Earth Syst. Sci. Discuss. 11 (2), 793–817.
Tor-ngern, P., et al., 2015. Increases in atmospheric CO2 have little influence on transpiration of a temperate forest canopy. New Phytol. 205 (2), 518–525.
Tuzet, A., Castell, J.F., Perrier, A., Zurfluh, O., 1997. Flux heterogeneity and evapotranspiration partitioning in a sparse canopy: the fallow savanna. J. Hydrol. 188 (1–4), 482–493.
Van Oijen, M., et al., 2011. A Bayesian framework for model calibration, comparison and analysis: application to four models for the biogeochemistry of a Norway spruce forest. Agric. For. Meteorol. 151 (12), 1609–1621.
Van Oijen, M., Rougier, J., Smith, R., 2005. Bayesian calibration of process-based forest models: bridging the gap between models and data. Tree Physiol. 25 (7), 915–927.
Wang, J., Wang, J., Ye, H., Liu, Y., He, H., 2017. An interpolated temperature and precipitation dataset at 1-km grid resolution in China (2000–2012). China Scientific Data 2 (1), 88–95.
Wang, K.C., Dickinson, R.E., 2012. A review of global terrestrial evapotranspiration: observation, modeling, climatology, and climatic variability. Rev. Geophys. 50, 54.
Wang, L., Good, S.P., Caylor, K.K., 2014. Global synthesis of vegetation control on evapotranspiration partitioning. Geophys. Res. Lett. 41 (19), 6753–6757.
Ward, E.J., et al., 2013. The effects of elevated CO2 and nitrogen fertilization on stomatal conductance estimated from 11 years of scaled sap flux measurements at Duke FACE. Tree Physiol. 33, 135–151.
Wei, Z.W., et al., 2017. Revisiting the contribution of transpiration to global terrestrial evapotranspiration. Geophys. Res. Lett. 44 (6), 2792–2801.
Wild, M., 2009. Global dimming and brightening: a review. J. Geophys. Res. 114 (D10), 1–31.
Wild, M., et al., 2009. Global dimming and brightening: an update beyond 2000. J. Geophys. Res. 114 (D10), 1–14.
Williams, et al., 2009. Improving land surface models with FLUXNET data. Biogeosciences 6, 1341–1359.
Wilson, K.B., et al., 2002. Energy balance closure at FLUXNET sites. Agric. For. Meteorol. 113 (1), 223–243.
Wilson, K.B., Hanson, P.J., Mulholland, P.J., Baldocchi, D.D., Wullschleger, S.D., 2001. A comparison of methods for determining forest evapotranspiration and its components: sap-flow, soil water budget, eddy covariance and catchment water balance. Agric. For. Meteorol. 106 (2), 153–168.
Woodward, F.I., 1990. Global change: translating plant ecophysiological responses to ecosystems. Trends Ecol. Evol. (Amst.) 5 (9), 308–311.
Xiao, Z., et al., 2014. Use of general regression neural networks for generating the GLASS leaf area index product from time-series MODIS surface reflectance. IEEE Trans. Geosci. Remote 52 (1), 209–223.
Xiao, Z., et al., 2016. Long-time-series global land surface satellite leaf area index product derived from MODIS and AVHRR surface reflectance. IEEE Trans. Geosci. Remote Sens. 54 (9), 5301–5318.
Yao, Y., et al., 2013. MODIS-driven estimation of terrestrial latent heat flux in China based on a modified Priestley–Taylor algorithm. Agric. For. Meteorol. 171 (2013), 187–202.
Zeng, Z., et al., 2014. A worldwide analysis of spatiotemporal changes in water balance-based evapotranspiration from 1982 to 2009. J. Geophys. Res. Atmos. 119 (3), 1186–1202.
Zhang, C., Chu, J.G., Fu, G.T., 2013. Sobol''s sensitivity analysis for a distributed hydrological model of Yichun River Basin, China. J. Hydrol. 480, 58–68.
Zhang, K., et al., 2017. Parameter sensitivity analysis and optimization for a satellite-based evapotranspiration model across multiple sites using Moderate Resolution Imaging Spectroradiometer and flux data. J. Geophys. Res. Atmos. 122 (1), 230–245.
Xiao, W., et al., 2018. Evapotranspiration partitioning at the ecosystem scale using the stable isotope method—a review. Agric. For. Meteorol. 263 (2018), 346–361.
Yuan, W.P., et al., 2010. Global estimates of evapotranspiration and gross primary production based on MODIS and global meteorology data. Remote Sens. Environ. 114 (7), 1416–1431.
Zhao, Y., et al., 2010. Modeling grazing effects on coupled water and heat fluxes in Inner Mongolia grassland. Soil Tillage Res. 109 (2), 75–86.
Zheng, H., et al., 2016. Spatial variation in annual actual evapotranspiration of terrestrial ecosystems in China: results from eddy covariance measurements. J. Geogr. Sci. 26 (10), 1391–1411.
Zhou, S., Yu, B., Zhang, Y., Huang, Y., Wang, G., 2016. Partitioning evapotranspiration based on the concept of underlying water use efficiency. Water Resour. Res. 52 (2), 1160–1175.
Zhou, S., Yu, B., Zhang, Y., Huang, Y., Wang, G., 2018. Water use efficiency and evapotranspiration partitioning for three typical ecosystems in the Heihe River Basin, northwestern China. Agric. For. Meteorol. 253–254 (2018), 261–273.
Zhu, G., et al., 2016a. Multi-model ensemble prediction of terrestrial evapotranspiration across north China using Bayesian model averaging. Hydrol. Process. 30 (16), 2861–2879.
Zhu, G., Su, Y., Li, X., Zhang, K., Li, C., 2013. Estimating actual evapotranspiration from an alpine grassland on Qinghai-Tibetan plateau using a two-source model and parameter uncertainty analysis by Bayesian approach. J. Hydrol. 476, 42–51.
Zhu, G.F., et al., 2014a. Simultaneously assimilating multivariate data sets into the two-source evapotranspiration model by Bayesian approach: application to spring maize in an arid region of northwestern China. Geosci. Model. Dev. 7 (4), 1467–1482.
Zhu, X.-J., et al., 2015. Spatiotemporal variations of T /ET (the ratio of transpiration to evapotranspiration) in three forests of Eastern China. Ecol. Indic. 52, 411–421.
Zhu, G.F., et al., 2014b. Simultaneously assimilating multivariate data sets into the two-source evapotranspiration model by Bayesian approach: application to spring maize in an arid region of northwestern China. Geosci. Model. Dev. 7 (4), 1467–1482.
Zhu, Z., et al., 2016b. Greening of the Earth and its drivers. Nat. Clim. Chang. 6 (8), 791–795.